Final Report to DOE

New Oxide Materials for an Ultra High Temperature Environment (DE-SC0010477)

PI: Professor John H. Perepezko
Department of Materials Science and Engineering
1509 University Avenue
Madison, WI 53706
Telephone: 608-263-1678
Email: perepezk@engr.wisc.edu

Background

Oxide formation in (Hf,Ta) solid solution alloys

There are a large number of ternary and higher order oxides involving two or more metal components. The multicomponent oxide structures develop at much higher additive levels than those typically involved in doping, but the structural modifications can also have a significant impact on oxygen transport. For example, in the case of transition metals, the characteristic multiple valence states are associated with different oxide structures. This characteristic behavior suggests a possible route to identify new high temperature oxides that can also inhibit oxygen transport in ultrahigh temperature ceramics.

In the case of Hf an early report by Marnoch [MAR65] on the oxidation of Hf-Ta alloys provided some intriguing results on enhancing oxidation resistance. The Hf-Ta system [KRI89] is characterized by a monotectoid isotherm reaction at 1083 °C and 40.3 wt pct. Ta. At elevated temperature there is a complete miscibility in the BCC phase. The melting points for Hf and Ta are respectively, 2231 °C and 3020 °C. With increasing alloying levels of Ta, Hf-Ta alloys exhibited an increasing oxidation resistance up to 27wt % Ta based upon metallographic study of oxidized sample cross sections. Neither the oxide structure nor the kinetic behavior were determined completely.
In preliminary work we have confirmed the early results as shown in figure 2 following a torch exposure to 1650° C for 10 min. There is a clear trend of decreasing oxide thickness with increasing Ta level up to 27wt %Ta. During oxidation a well bonded oxide develops that shows thermal shock resistance and freedom from breakaway failure modes. Moreover, the micrographs of oxidized sample cross sections in figure 3 reveal the development of an intermediate reaction zone between the outer surface oxide and the alloy substrate. X-ray diffraction (XRD) analysis was employed to identify the structure in the reaction zone product. The XRD analysis in figure 4a shows that with increasing Ta level the oxide changes from monoclinic HfO_2 to a series of complex orthorhombic ternary oxides such as $Hf_7Ta_2O_{19}$ with reduced mobility for oxygen transport as illustrated in figure 4b [SPI81]. This is a new result that appears to be a key factor in the improved oxidation performance. Marnoch suggested that the improvement in the oxidation resistance could be attributed to the denser formation of Hf-Ta solid solution oxide [MAR65] which limits the oxide growth rate. Recently, the Hf-based metallic coatings have been successfully applied to carbon composites where the oxidation resistance up to 1850^{o}C is dramatically increased by tantalum addition [AND12]. It is not clear however as to the mechanism by which tantalum can be added into Hf-based known oxides (which include monoclinic, tetragonal as well as cubic structural variants) as there is very limited available data on the pseudo-binary of $HfO_2 - Ta_2O_5$. It has been known however that there is a limited solubility tantalum in monoclinic HfO_2 [SPI81]. Our preliminary work suggests that the improvement in the oxidation resistance is also accompanied the conversion of the monoclinic HfO_2 into a series of homologous $Hf_{½(n-5)}Ta_2O_n$ (n=15,17 and 19) oxide structures. For simplicity in the following discussion the homologous $Hf_{½(n-5)}Ta_2O_n$ (n=15,17 and 19) oxide structures will be described by HfTaO oxide superstructures.

The oxidation tests proved that the Ta additions significantly reduce the oxide thickness in Hf-Ta alloys. The XRD results demonstrate that Hf-Ta alloys oxidized at 1200°C-1650 °C form monoclinic HfO_2 and/or orthorhombic $Hf_7Ta_2O_{19}$. The preliminary findings also show that the "Ta effect" is not due to doping into the monoclinic-HfO_2, but rather it is due to the large accommodation of tantalum substitution for Hf in HfO_2 with the α-PbO_2 prototype crystal structure. As explained later, the large incorporation of Ta in the complex oxides facilitates a defect structure that inhibits oxygen mobility. The initial kinetics analysis in [MAR65] and our work suggests a parabolic dependence of oxide thickness with time over at 1200 and 1300°C indicating a volume diffusion governing the O transport in the Hf-Ta complex oxides. Clearly, a complete kinetics analysis over a wide temperature range is warranted to establish the enhanced oxidation performance. Since the Zr-Ta system has a similar phase diagram as Hf-Ta alloys and ZrO_2 shows similar structures as HfO_2, it is reasonable to expect a similar homologous series of Zr-Ta oxide

superstructures. In this case the incorporation of Ta in ZrB_2 to form $(Zr,Ta)B_2$ can be expected to develop complex Zr-Ta oxides with low oxygen mobility instead of ZrO_2 which has a high oxygen mobility.

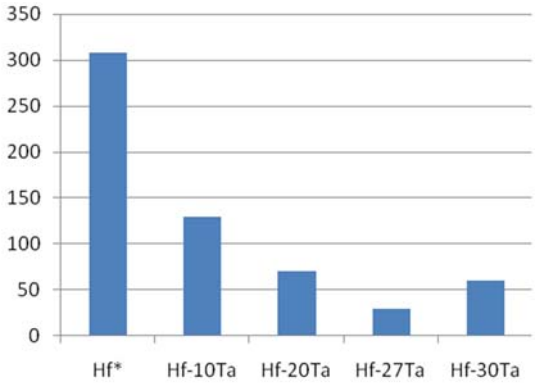

Figure 1. Oxide scale thickness (μm) for 1650°C torch exposure showing the effect of Tantalum substitution for Hf in Hf-Ta alloys. (* Hf oxidation is estimated from the previous kinetic study at high temperatures [KOF67]

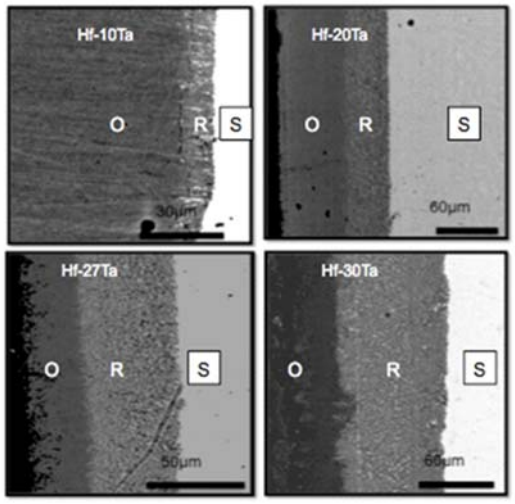

Figure 2. Torch 1650°C exposure-sample cross section (O-oxide scale, R-reaction zone, S-substrate).

Phase Stability in HfO_2/ZrO_2 with α-PbO_2 Prototype

It is useful to evaluate the thermodynamic stability of the HfO_2 phase that adopts the α-PbO_2 crystal structure instead of the stable monoclinic structure. The stability of the homologous series of Hf/Zr-rich Hf-Ta oxides, can be examined in terms of the stability of the prototype structures of HfO_2/ZrO_2. The α-PbO_2 structure, one of the possible metastable phases, has long been argued to be in close competition with the monoclinic structure according to the results from DFT calculations at the ground state (O K). In fact, the DFT calculations show that the HfO_2 phase that adopts the α-PbO_2 crystal structure has a much lower energy than that of the tetragonal as well as the cubic structures (known crystal variants) of HfO_2. Nevertheless, the existence of an α-PbO_2 type of HfO_2 has been very difficult to prove experimentally.

a)

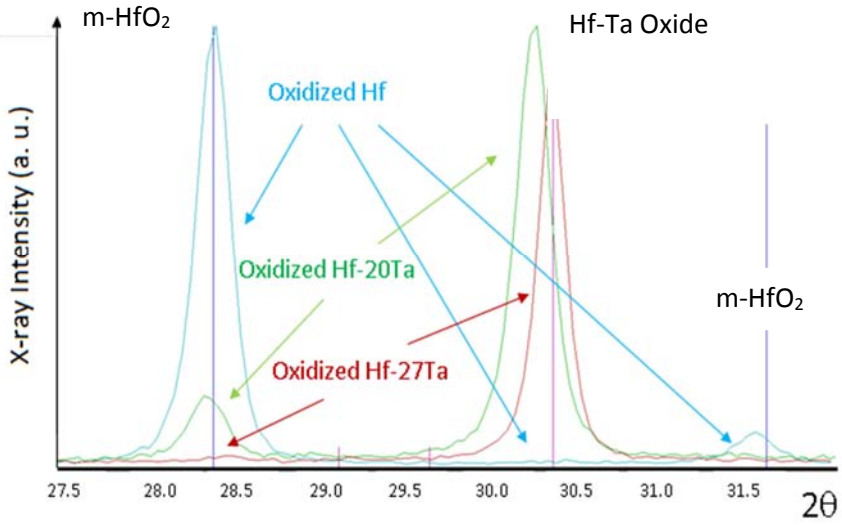

b)

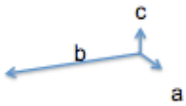

$Hf_7Ta_2O_{19}$

Crystal Structure : Orthorhombic a = 0.49 nm, b = 9.7 nm and c = 0.52 nm

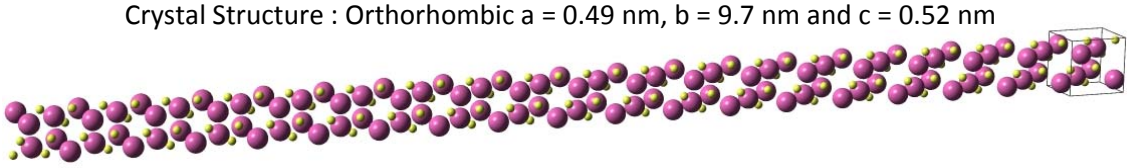

$Hf_6Ta_2O_{17}$

Crystal Structure : Orthorhombic a = 0.49 nm, b = 8.7 nm and c = 0.53 nm

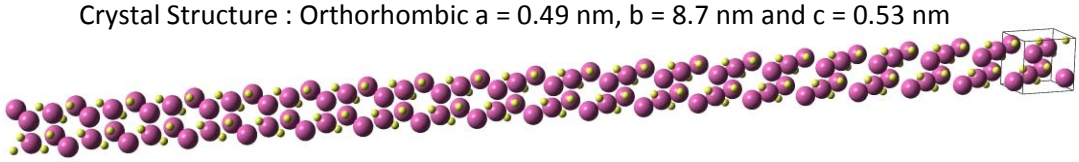

$Hf_5Ta_2O_{15}$

Crystal Structure : Orthorhombic a = 0.49 nm, b = 7.7 nm and c = 0.53 nm

Figure 3a) XRD of oxidized Hf, Hf-Ta alloys at 1200°C showing the disappearance of the monoclinic m-HfO_2 and the formation of orthorhombic Hf-Ta oxides as shown in (b). Hf-Ta oxides are stable with crystal structures that follow a homologous series of superstructures from an orthorhombic α-PbO_2 crystal prototype with number of multiplication factors (15, 17, and 19) in the b axis direction. Incorporation of each Ta ion (5+) is assumed to result in a hole which is balanced by the formation of cation vacancy ("cation-poor"). The crystal structure is based on the alpha lead oxide (α-PbO_2) prototype but forms as a superstructure with a repeat unit in the b axis direction.

Homologous Series	N	Estimated Crystal Volume ($Å^3$)
$Hf_5Ta_2O_{15}$	15	**32.7**
$Hf_6Ta_2O_{17}$	17	**33.2**
$Hf_7Ta_2O_{19}$	19	**33.1**

Table 1 Crystal volume of the homologous series normalized to one 'molecule' of HfO_2 in the α-PbO_2 crystal structure

It was argued that this may be due to the fact that to transform the monoclinic (or even cubic/tetragonal) structure of HfO_2 into the α-PbO_2 structure, a negative pressure (volume expansion) is required as noted in the recent DFT work on HfO_2 (figure 5). Using curve fitting procedures and following a Murnaghan Equation of State (EOS) equation as depicted in figure 5 by the curves for each of the possible crystal structures, one can see that the most stable crystal structure is the monoclinic phase with the lowest total energy of ~ 30.55 eV and a crystal volume of 34.8 $Å^3$. While the second most stable structure is alpha PbO_2 with a total energy of -30.5 eV and a crystal volume of 37.4 $Å^3$, its minimum energy resides at a higher volume crystal structure. This means that to transform the monoclinic HfO_2 structure into the α-PbO_2 crystal structure there must be a volumetric expansion.

The existence of the homologous series suggests that the introduction of tantalum may promote the thermodynamic stability of the α-PbO_2 relative to that of the monoclinic or tetragonal or cubic phase. Table 1 shows the crystal volume normalized to one unit cell of PbO_2 for the homologous series crystal structures described previously. Thus, the introduction of Ta ion results in the lowering of the effective volume surrounding the HfO_2 within the crystal structure. Indeed, it is not clear if this reduction is also accompanied by the development of the energetically unfavorable α-PbO_2 versus the stable monoclinic crystal variant.

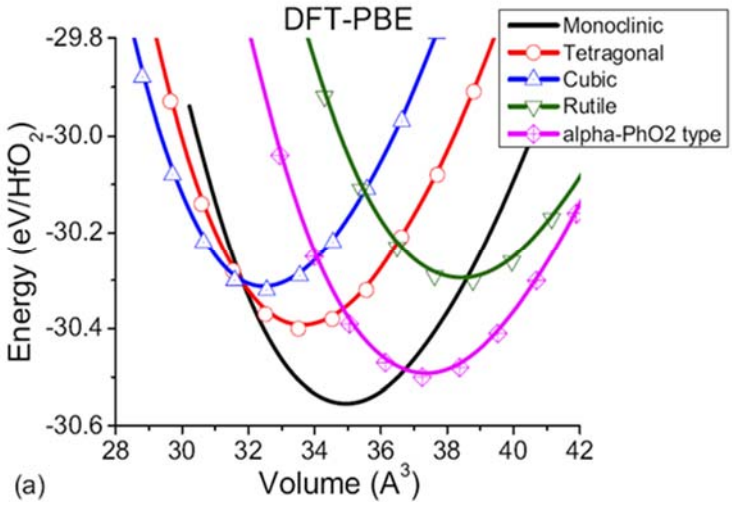

Figure 4 Comparison of the energy of formation of HfO_2 adopting various types crystal structures based on the DFT- calculations [TER08] under Perdew, Burke, and Ernzerhof (PBE) generalized gradient approximation[PER96].

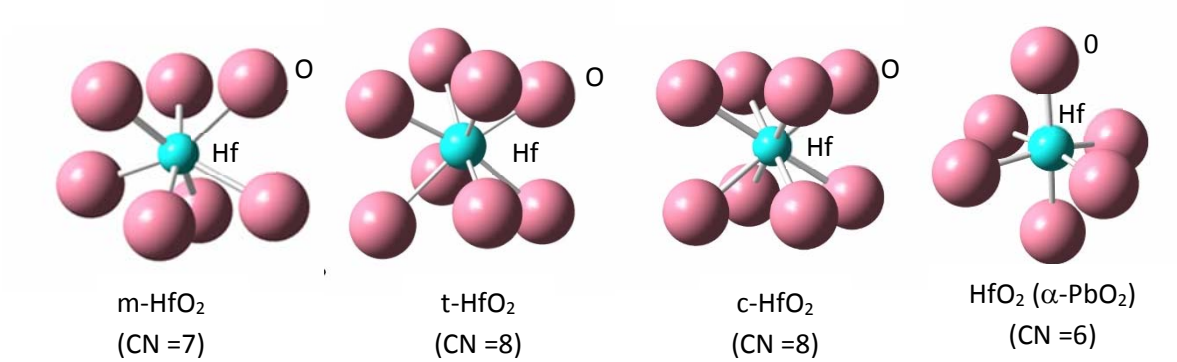

Figure 5 The Hf-O cluster configuration in the HfO_2 crystal structure in a) monoclinic, b)tetragonal, c)cubic and α-Pb-O_2 prototypes. The higher the CN in HfO_2, the higher contribution of the covalence (pd hybridization) to the Hf-O bonding [TER08]. The α-PbO_2 structure has the lowest coordination number (CN=6) amongst the four crystal variants and has the most charge transfer from Hf to its surrounding oxygen anions.

While it is evident that all of the homologous crystal structures have crystal volumes that are larger than that of monoclinic HfO_2 which may permit the phase transformation to take place experimentally, it not clear however as to why the energetics of the α-PbO_2 structure becomes favored with Ta addition. Thus, a systematic study and model on thermodynamic stability of these oxides are warranted. More importantly it is essential to identify the governing defect structures within the oxides. The types of governing defect structures in transition metal oxides in general can be strongly affected by the oxygen partial pressure and temperature. For example, at a low partial pressure of oxygen, the major defect structures in Ta_2O_5 are controlled by oxygen vacancies and electrons whereas at a high partial pressure of oxygen, the major defects are oxygen interstitials and electron holes [STR74][RAM03]. There has not been a systematic study both theoretical as well as experimental in evaluating the thermodynamic stability of the homologous oxide series.

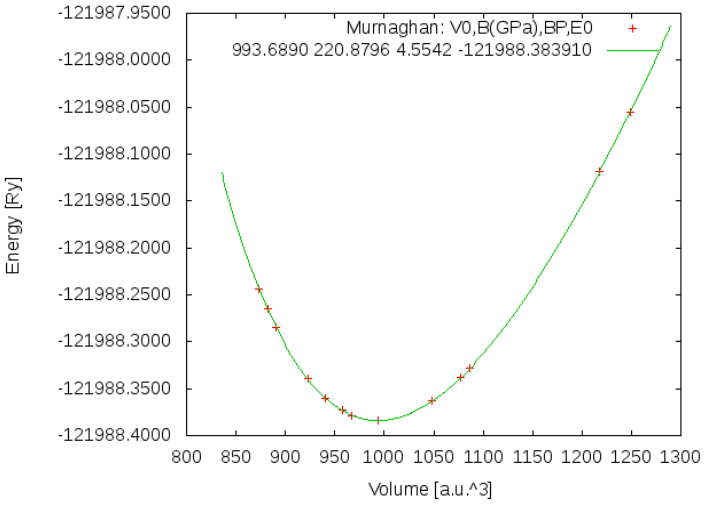

Figure 6 The preliminary result of DFT calculations on HfO_2 (α-PbO_2) showing the total energy of as a function of unit volume with a calculated Bulk Modulus (based of EOS) of 220.9 MPa.

Preliminary DFT-based phase stability analysis on the stability of alpha-PbO_2 crystal structure of HfO_2 suggests that unlike cubic, tetragonal or even monoclinic crystal variants of HfO_2 that are characterized by a mixed covalent and ionic Hf-O bonding , the α-PbO_2 structure adopts a more ionic bonding. This can be understood from the ionic Hf-centered O clustering that is available to these crystal variants (figure 6). The monoclinic structure, which is the most stable at low temperature (up to 2000 K) has a coordination number of 7. Previous study shows that while most of the chemical bonding is ionic in character, there is a covalent, charge-sharing along the Hf-O directions [TER08]. This partly covalent bonding becomes even more pronounced in the tetragonal and cubic crystal variants of HfO_2 due to the corresponding increase in the coordination number to 8 (for both crystals). The α-PbO_2 structure on the other hand adopts a 6 CN which results in a strong ionic character of its Hf-O bonding. Further, analysis on the bulk modulus of the HfO_2 with the α-PbO_2 crystal variant shows a lower value (~ 221 MPa) than that reported for monoclinic

as well as tetragonal and cubic variants of HfO_2 (B= 249 MPa, 235MPa, 233 MPa for cubic, tetragonal and monoclinic HfO_2 respectively[TER08]) . Figure 7 shows the fitting of Murnaghan's equation of state (EOS) of the α-PbO_2 crystal variant which yields the lower bulk modulus, indicative of the weakening of the directional bonding as the charge density of the valence states is partly transferred to the interstitial regions and oxygen anions. The relatively stronger ionic character of Hf-O bonding in the α-PbO_2 prototype may also suggest that the HfO_2 (α-PbO_2) structure is much more receptive to defect engineering to influence the oxygen transport by for example the Ta to Hf cation substitution.

Summary

In this project, a new oxide material, $Hf_6Ta_2O_{17}$ has been successfully synthesized by the controlled oxidization of Hf-Ta alloys. This oxide exhibits good oxidation resistance, high temperature phase stability up to more than 2000°C, low thermal conductivity and thus could serve as a component or a coating material in an ultrahigh temperature environment. We have examined the microstructure evolution and phase formation sequence during the oxidation exposure of Hf-Ta alloys at 1500°C and identified that the oxidation of a Hf-26.7atomic %Ta alloy leads to the formation of a single phase adherent $Hf_6Ta_2O_{17}$ with a complex atomic structure i.e. superstructure. The overall reactive diffusion pathway is consistent with the calculated Hf-Ta-O ternary phase diagram. Besides the synthesis of $Hf_6Ta_2O_{17}$ superstructure by oxidizing Hf-Ta alloys, we have also developed a synthesis method based upon the reactive sintering of the correct ratios of mixed powders of HfO_2 and Ta_2O_5 and verified the low thermal conductivity of $Hf_6Ta_2O_{17}$ superstructure on these samples. We have completed a preliminary analysis of the oxidation kinetics for $Hf_6Ta_2O_{17}$, which shows an initial parabolic oxidation kinetics.

Main Goals

The proposed study includes the systematic fundamental study of the structure synthesis, phase stability and oxidation reaction kinetics. We have achieved most of the proposed goals. For structure synthesis of HfTaO structure, we have developed two methods to synthesize the superstructure, one is synthesized by controlled oxidation of Hf-Ta alloy and the other one is synthesis through pure HfO_2 and Ta_2O_5. We have also added understanding of the reaction path for the synthesis of the HfTaO superstructure from both an experimental approach and a thermodynamic evaluation. For phase stability, we have examined the phase stability of HfTaO superstructure and verified that the HfTaO superstructure is stable until 2004°C. We also examined the phase stability of other phases shown in system. For oxidation kinetics, we have verified that the HfTaO superstructure has good oxidation resistant properties and identified the parabolic oxidation kinetics of the HfTaO superstructure coated on Hf-Ta alloys.

Project activities

In this project, we have made progress in achieving the main objectives as identified in the following.

1. Oxidation synthesis of HfTaO superstructure.
   The XRD pattern and microstructures of as-cast samples are shown in Fig. 7. After oxidation exposure the oxide scale appeared to adhere well without spallation for all samples. The XRD patterns to determine the oxidation products for the Hf-Ta alloys are presented in Fig.3. For the Hf-19.7Ta alloy oxidation yields a mixture of the HfTaO superstructure and monoclinic HfO_2. For the Hf-49.6Ta alloy oxidation results in a mixture of HfTaO superstructure and Ta_2O_5. Both Hf-26.7Ta and Hf-34.7Ta alloy XRD patterns reveal a pure HfTaO superstructure pattern, however, according to Spridonov et. [14], the range of Hf:Ta ratio in HfTaO superstructure is 2.5 to 3.5, which is too high for Hf-34.7Ta alloy to form a single phase superstructure. If Hf:Ta ratio is treated as the phase boundary for the HfTaO superstructure and it is assumed that there is negligible HfO_2 or Ta_2O_5 solubility in the HfTaO superstructure, then some excess Ta oxide will form during the oxidation of Hf-34.7Ta. However, according to the range of the Hf:Ta ratio in the HfTaO superstructure, the amount of Ta oxide is about 0.8%, which is too low for detection by XRD. Thus, pure HfTaO superstructure can be synthesized by oxidizing the Hf-26.7Ta alloy.
   For Hf-Ta alloys with excess Hf, the oxide scale is composed of $Hf_6Ta_2O_{17}$ and monoclinic HfO_2, while for Hf-Ta alloys with excess Ta, the oxide scale is composed of $Hf_6Ta_2O_{17}$ and orthorhombic Ta_2O_5.

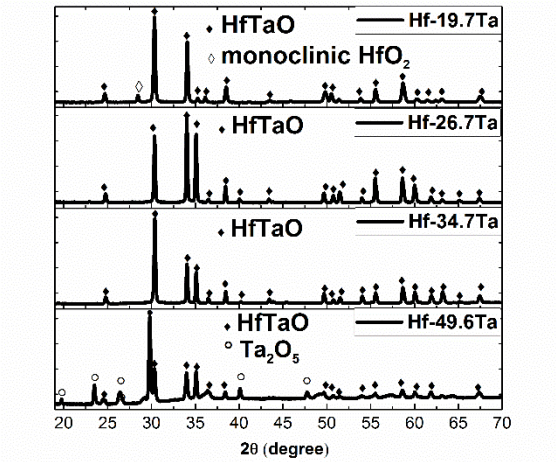

Fig. 7 XRD pattern of oxides formed by oxidizing Hf-Ta alloys with different compositions.

2. Oxidation resistant properties of HfTaO superstructure.
   The cross section microstructures of the oxidized samples in Fig. 8 (a) – (d) present an overview of the relative reaction rates as a function of composition following oxidation exposure. A more detailed view of the microstructure developed at the substrate/ reaction layer interface and the reaction layer/oxide interface is given in Fig. 8(e) and (f)

respectively. It is evident that along the oxygen diffusion direction, all samples exhibit a three-layer microstructure represented by an oxide layer, a reaction layer and the substrate. For samples with different compositions, the thickness and microstructure of each layer are different.

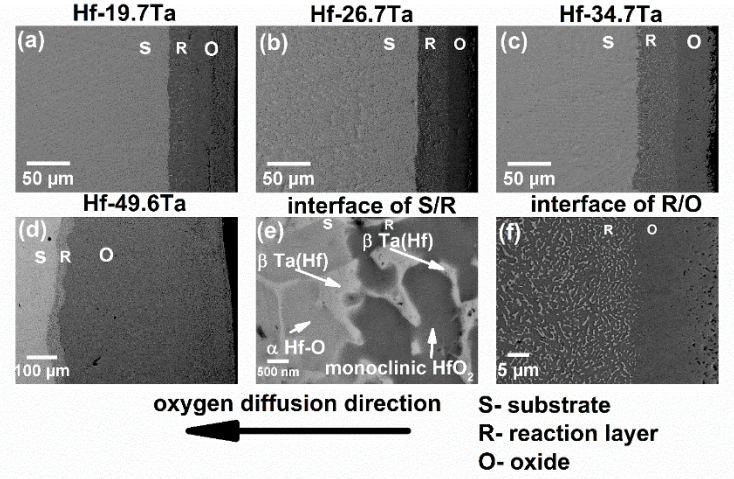

Fig. 8 Cross section view of oxidized (a) Hf-19.7Ta, (b) Hf-26.7Ta, (c) Hf-34.7Ta, (d) Hf-49.6Ta and the interface of (e) substrate/ reaction layer and (f) reaction layer/oxide.

The sum of the thicknesses of the reaction layer and the oxide layer can be took as an indication of oxidation- resistance behavior (Fig. 9). With increasing Ta concentration, the sum of oxide thickness and reaction layer thickness decreases first, reaches a minimum at Hf-26.7Ta, then increases up to Hf-49.6Ta. While the oxide layer of the Hf- 26.7Ta alloy is pure HfTaO superstructure, the layer for the other compositions is a mixed phase layer. Thus, the oxidation of the Hf-26.7Ta alloy that leads to the formation of pure HfTaO superstructure also has the best oxidation- resistance behavior among the Hf-Ta alloys.

The superior oxidation resistant properties of the Hf-26.7Ta alloy is attributed to the compact oxide scale of $Hf_6Ta_2O_{17}$, which adheres well with the alloy substrate. With this observation and the identified reaction pathway, the diffusion of oxygen through the scale is the rate-limiting factor for the oxidation and superstructure synthesis.

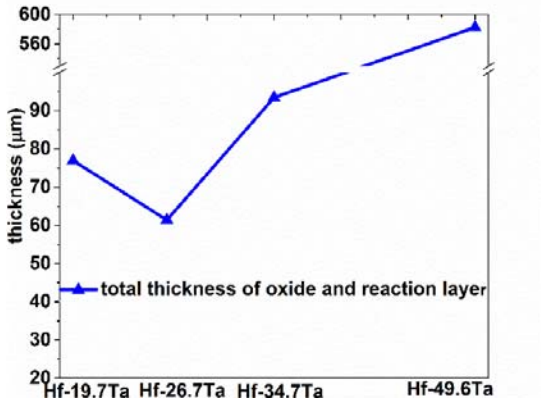

Fig. 9 Oxygen penetration depth of Hf-Ta alloys with different compositions.

3. Analysis of the reaction path during the formation of HfTaO superstructure

In order to document the reaction path for the formation of the $Hf_6Ta_2O_{17}$ superstructure, a Hf-26.7Ta sample which was oxidized at 1500°C for 10min was polished carefully from surface down to the substrate. After each polishing increment of around 10μm, XRD (Fig. 10) and SEM (Fig. 11) was used to examine the phase identity and microstructure of the exposed layer. From the XRD and SEM examination of the surface, it is confirmed that the oxide is the HfTaO superstructure. After removal of around 10μm, the oxide is still characterized as HfTaO superstructure (not shown in Fig. 10). After another ~20μm removal to reach the interface of the oxide layer and the reaction layer, the microstructure (Fig. 11 (a)) revealed small bright β Ta(Hf) rich regions rather than a single phase oxide. The XRD pattern indicated that there are three phases at this level, which are the monoclinic HfO_2, the HfTaO superstructure and the β Ta(Hf) solid solution. However, in the enlarged view in portion of Fig. 11(a) that is shown in Fig. 11(b), it is apparent from the contrast variation that the HfO_2 and β Ta(Hf) phases are undergoing a reaction. Upon moving 10μm further into the reaction layer near the oxide/reaction layer interface, the relative intensity of XRD peaks belonging to the HfTaO superstructure decreased and finally vanished while there is an increase in the peak intensity for the monoclinic HfO_2 phase. Moreover, an increase in phase content of the β Ta(Hf) phase was also detected in the XRD pattern. The microstructures of these layers (Fig. 11 (a)-(d)) confirm this result, it is seen that the bright Ta-rich phase is increasing in amount. When the polishing reached the reaction layer/substrate interface, besides the monoclinic HfO_2 pattern and the β Ta-Hf phase pattern, there is an indication for the α Hf-O phase. Thus, the α Hf- O phase is oxidized as monoclinic HfO_2 while the β Ta(Hf) phase is not oxidized at this interface. This result is consistent with the previous result shown in Fig. 8(e) and is also evident in Fig. 11 (e). The XRD result indicates that the substrate adjacent to the interface is composed of the α Hf-O phase and β Ta(Hf) phase, which is also confirmed by the microstructures shown in Fig. 11(f).

To investigate the composition change in each layer involved in the oxidation process, several EPMA line scans were conducted to obtain a composition profile across the oxidized Hf-26.7Ta sample as presented in Fig. 12(a). The line scan was conducted parallel to the oxygen diffusion direction to determine the composition change from the external oxide to the substrate. It is evident from the composition profile of scan 1 that along the oxygen diffusion direction, there are three distinct sections of the composition profile which correspond to the oxide, the reaction layer and the substrate as shown in the cross section microstructures.

The composition levels of Hf, Ta and O are all relatively stable with average of 23.8 ± 0.7 at.%, 8.20 ± 0.5 at.% and 68.0 ± 1.1at.%, which indicates that the $Hf_6Ta_2O_{17}$ superstructure is present in the first 25μm of the oxide layer. It is worthwhile to note that from 25μm to 30μm into the sample the oxygen composition is decreasing from around 68 at.% to 62 at.% and the composition of Hf is observed to increase from 25 to about 30 at.%. In order to account for this composition profile we note that the α Hf-O solid solution is oxidized as HfO_2,and the β Ta(Hf) solid solution phase is not oxidized, but contains around 9 at.% Hf according to calculated Hf-Ta-O phase diagram shown in Fig. 14. Based on initial composition of Hf-26.7Ta alloy, the phase amounts in this region are 70.66% HfO_2 and 29.34% β Ta Hf solid solution. Thus, the oxygen composition should be 58.56%. However,

the oxygen level changed from 68 to 62 at.%, which is larger than 58.56%. This result suggests that the β Ta(Hf) is initially oxidized as a metastable Ta oxide rather than the stable Ta_2O_5.

In reaction layer, the composition of O, Hf and Ta are relatively stable with some fluctuations due to the two-phase mixture of HfO_2 and β Ta(Hf) phase. The composition profile of Hf, Ta and O change dramatically across the interface of reaction layer and substrate.

Based on the experimental results from the oxidation of Hf-Ta alloys with different compositions, it was determined that the Hf-26.7Ta alloy has superior oxidation resistance among all Hf-Ta alloys and develops a pure $Hf_6Ta_2O_{17}$ phase as the oxide scale. The reaction path that leads to the formation of the $Hf_6Ta_2O_{17}$ superstructure phase has been identified, as:

β Hf-Ta solid solution → HCP α Hf-O solid solution + Ta rich β Ta(Hf) solid solution → monoclinic HfO_2 + Ta rich β Ta(Hf) solid solution → monoclinic HfO_2 + metastable Ta oxide/(Hf, Ta)O solid solution → $Hf_6Ta_2O_{17}$

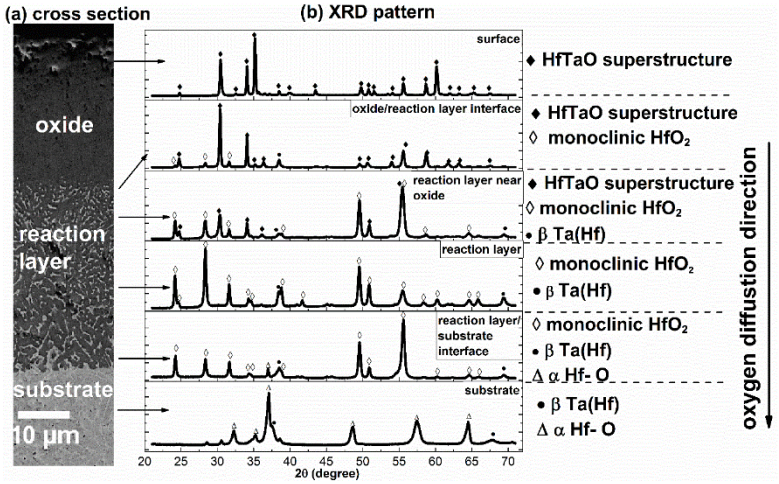

Fig. 10 XRD depth profile of oxidized sample

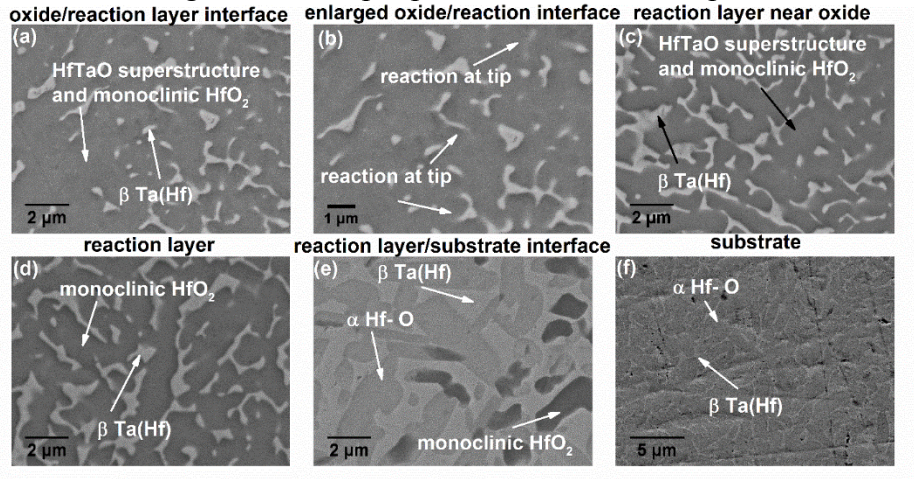

Fig. 11 Plan view acquired at exposed plans shown in Fig. 5. (a) oxide/reaction layer interface, (b) enlarged oxide/reaction layer interface, (c) reaction layer near oxide, (d) reaction layer, (e) reaction layer/substrate interface, (f) substrate.

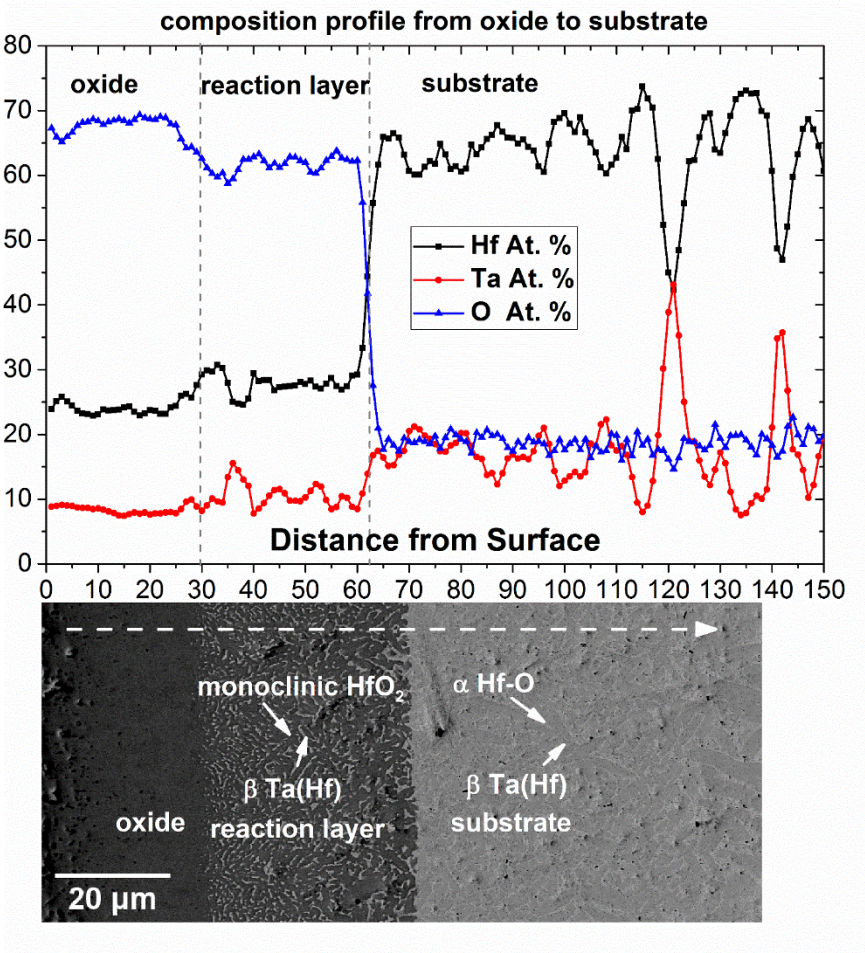

Fig. 12 Composition profile from oxidized surface to substrate of a Hf-26.7Ta alloy oxidized at 1500°C for 10min.

4. Thermodynamic evaluation of the Hf-Ta-O ternary system and identification of the reaction path to form HfTaO.

To assist in the interpretation of the superstructure synthesis reaction pathway during oxidation, the calculated Hf-Ta-O isothermal section at 1500°C is useful. The calculated Hf-Ta-O isothermal section at 1500ºC using Pandat™ and a self-consistent Hf-Ta-O thermodynamic database is shown in Fig. 13. While thermodynamics determines what phases can coexist when equilibrium conditions are achieved, it does not determine what combinations of phases may form in the process of achieving equilibrium. The intermediate phase sequences are mainly determined by kinetics. For example, the condition for the formation of the layered structure is that the diffusivity of one of the component elements within the diffusion zone is much higher than that of other component elements. This is the case in the current work since the diffusivity of oxygen is much greater than those of Hf and Ta. As shown in Figure 13, the star symbol is the substrate composition Hf-26.7Ta. When we draw a dashed line to connect the Oxygen and the star, it will cross a few phase regions. These crossing phase regions indicate the possible phase layers can form during oxidation of the substrate. However, the layer forming sequence represents a specific

arrangement of phases in the oxygen/Hf-26.7Ta diffusion couple, in which each phase is in thermodynamic equilibrium with its neighboring phases. Thus, the experimentally observed oxide layers along the oxidation direction are single-phase regions, and boundaries between different layers correspond to the two-phase regions. No three-phase region can be observed, because the real diffusion path will go around the one of the boundaries of the tie-triangle rather than pass through it. Therefore, the phases involved in the previous two-phase region are subtracted from the three-phase regions. Once we could bridge the gap between different phase-regions as shown above, that will be the "real" phase layer sequence in the oxide scale. In order to do that, we need to consider the following theoretical rules as well: (a) Neighboring phases must be connected by a tie-line in the isothermal section, which is required when two phases are in equilibrium from the thermodynamic point of view; (b) The real oxidation/diffusion path much cross the straight line connecting the terminal compositions at least one, which is require to obey the mass balance rule; (c) The chemical potential of the major diffusing specie must intrinsically decrease, which is the driving force of this kinetic processing.

From the detailed microstructure analysis, the oxidation of Hf-Ta alloys and the formation of the HfTaO ($Hf_6Ta_2O_{17}$) superstructure include a series of intermediate processes that are illustrated schematically in Fig. 14. The observed reaction sequences leading to the formation of the $Hf_6Ta_2O_{17}$ superstructure and the layered oxidation synthesized microstructure are shown further on the calculated Hf-Ta-O isothermal phase diagram section at 1500°C in Fig. 13. With an initial substrate composition of Hf- 26.7at.%Ta the incorporation of oxygen results in the precipitation of the α-HfO phase in the β HfTa solid solution and the enrichment in Ta of the original β HfTa solid solution. One stage in this process is shown as in Fig. 14. The reaction continues with the addition of oxygen until the α-HfO phase is saturated at about 20 at.%O and in equilibrium with the β phase with about 9 at.% Hf and negligible oxygen in solution. Subsequent conversion of the α-HfO saturated phase into monoclinic HfO_2 establishes a (HfO_2 + βTa(Hf)) two phase equilibrium that is maintained until the BCC β Ta(Hf) phase is oxidized to Ta_2O_5. The last step in the reaction involves the reaction between HfO_2 and Ta_2O_5 to establish the three phase equilibrium with the $Hf_6Ta_2O_{17}$ superstructure. The outer $Hf_6Ta_2O_{17}$ superstructure layer is then in equilibrium with the gas phase. With this equilibrium reaction pathway the $Hf_6Ta_2O_{17}$ superstructure formation can be described by:

$$xHfO_2 + Ta_2O_5 \rightarrow xHfO_2 \cdot Ta_2O_5 \ (x=5, 6, 7)$$

However, from the examination of the phase evolution with depth by XRD no evidence was found for the development of the stable Ta_2O_5 phase in the reaction layer. Moreover, across the interface between the reaction layer and the $Hf_6Ta_2O_{17}$ superstructure outer layer the oxygen level changed from about 62 at.%O in the reaction layer to about 68 at% O in the $Hf_6Ta_2O_{17}$ layer. This region also correspond to the region in Fig. 11(b) where a reaction is observed between the HfO_2 and β Ta(Hf) phase. While the oxygen level in the outer layer matches the $Hf_6Ta_2O_{17}$ composition, the oxygen level in the reaction layer is well below the level required for Ta_2O_5 and well above the level for no β Ta(Hf) phase is oxidized. This suggests that an intermediate metastable Ta oxide reacts with the monoclinic HfO_2 to yield the $Hf_6Ta_2O_{17}$ superstructure. In fact, Ta is well known to exhibit a series of several intermediate oxides with variable stoichiometry during oxidation until formation of the stable Ta_2O_5 structure. One of these intermediates is $TaO_{0.88}$ with a cubic structure

that can meet the observed oxygen concentration level, but the identification of the specific Ta oxide form requires further study.

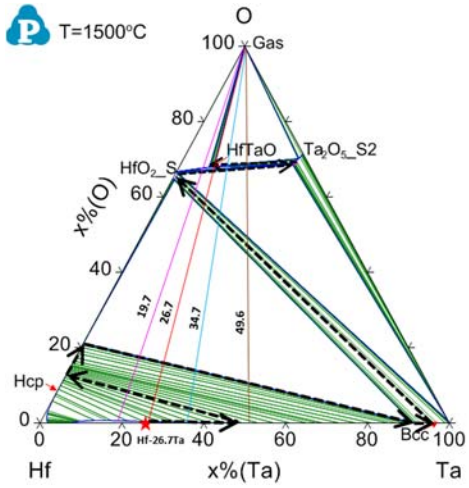

Fig. 13 Thermodynamic evaluation of Hf-Ta-O ternary system and the reaction path leading to the formation of the HfTaO superstructure.

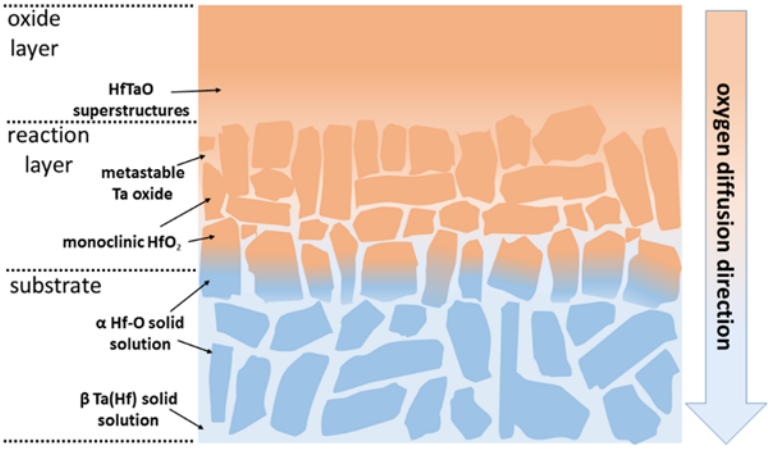

Fig. 14 illustration of oxidation process for Hf-Ta alloys.

5. Phase stability of the HfTaO superstructure

The high temperature phase stability of HfTaO superstructure was evaluated by DTA analysis (Netzsch) from 800°C to 2400°C. It is seen from the DTA trace that the HfTaO superstructure remains stable until the melting temperature at 2004°C. This result indicate that HfTaO superstructure has very good high temperature phase stability and suitable to be used at high temperature.

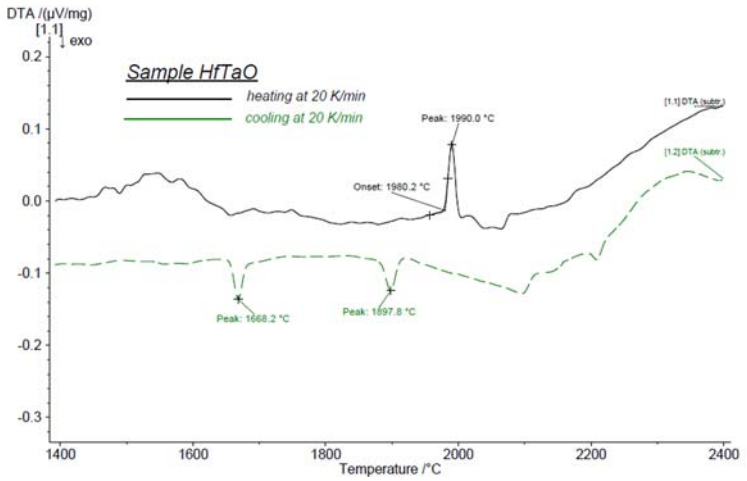

Fig. 15 DTA analysis of HfTaO superstructure from 800°C to 2400°C

6. Psudobinary phase diagram of HfO_2 – Ta_2O_5
   To enhance the understanding of Hf-Ta alloy oxidation and the phase relation during the formation of HfTaO superstructure, we also developed an HfO_2-Ta_2O_5 psudo-binary system from both experimental measurements and thermodynamic evaluation, as shown in Fig. 16.

   The XRD results for sintered powders with different ratios of HfO_2 and Ta_2O_5 is summarized as follows. Given the knowledge that the sintering of HfO_2 and Ta_2O_5 with ratio of 6:1 can lead to the formation of pure superstructure, the sintering of mixed HfO_2 and Ta_2O_5 with different ratio can give us some preliminary results of HfO_2 – Ta_2O_5 psudobinary phase diagram and the range or phase boundary of the superstructure phase.

   The sintering of the mixed powders was conducted at 1650°C for 24 hours, thus, the phases shown in samples is a reflection of the phase relation at 1650°C. However, to our best knowledge, there is no phase transformation for HfTaO superstructure and HfO_2 from room temperature to 1650°C. However, for Ta_2O_5, there is a phase transformation at 1320°C, thus, it is not surprising if we find some low temperature phase of Ta_2O_5.

   The XRD patterns of sintered mixed powders are shown in Fig. 17 (a). It is evident that for the 100:1 sample, the phases are a mixture of the monoclinic HfO_2 and the HfTaO superstructure. Only a trace of the HfTaO superstructure is detected, however, this is enough to determine that there is two phase field in the HfO_2-Ta_2O_5 system at this mole fraction. With increasing Ta_2O_5 mole fraction from the 0.99% to 12.5%, it is seen that the peaks for the HfTaO superstructure are increasing in intensity while the peaks for the monoclinic HfO_2 are decreasing, which indicates that the phase content of HfTaO superstructure is increasing and the monoclinic HfO_2 is decreasing. When the mole fraction of Ta_2O_5 is increased to 13.33%, it is seen from the pattern that there is no trace for the monoclinic HfO_2, which indicates that the sintered powder is pure superstructure. With the continued increase in the Ta_2O_5 content from 13.33% to 14.29%, the sintered powders are also pure HfTaO superstore. However, for a Ta_2O_5 content at 15.38%, a trace of Ta_2O_5 is identified and with increasing Ta_2O_5 content to 16.67%, that peaks for Ta_2O_5 increase in intensity. Therefore, from the phase determination of sintered samples with different Ta_2O_5

content, we can conclude that there is a single phase HfTaO superstructure region in HfO_2-Ta_2O_5 psudobinary phase diagram. The HfTaO superstructure can form a two phase field with both HfO_2 and Ta_2O_5, which indicates that there is no other compounds in this pseudobinary system.

In the pseudo-binary phase diagram, the composition range of HfTaO superstructure is identified, it is also identified that there is no solubility of HfTaO phase in HfO_2 but a large solubility of HfO_2 in Ta_2O_5. We are still performing experiments to complete this phase diagram by solid experiments support and to use the experimental resut to refine the phase diagram calculation..

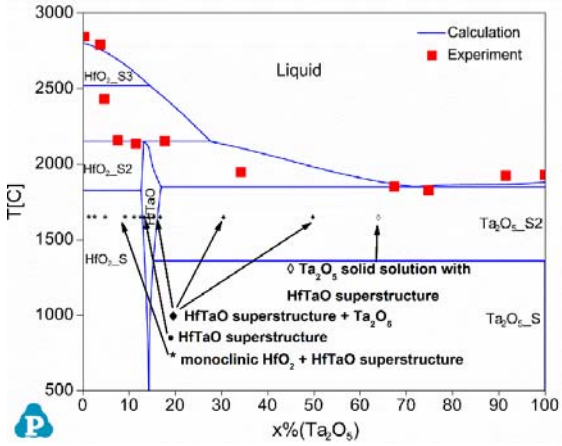

Fig. 16 HfO_2-Ta_2O_5 pseudobinary phase diagram.

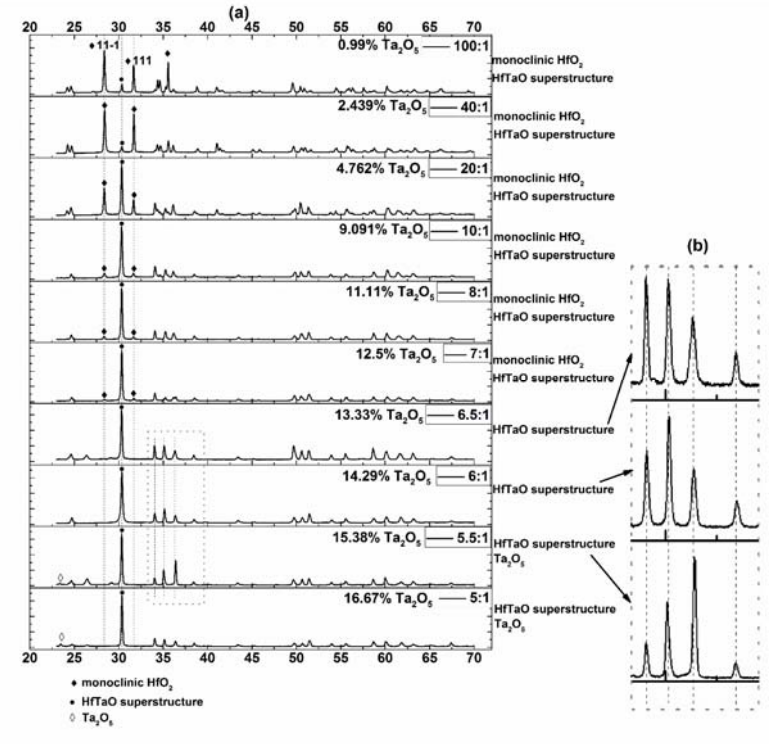

Fig. 17 (a) XRD pattern of sintered mixed HfO_2 Ta_2O_5 with different ratios, (b) enlarged view of peaks in grey rectangle.

The XRD patterns of sintered mixed powders on the Ta_2O_5- rich side are shown in Fig. 18. It is evident that the HfO_2: Ta_2O_5 2:1 sample and 1:1 sits in two phase region, which is indicated by HfO_2-Ta_2O_5 in the pseudobinary phase diagram. However, for HfO_2:Ta_2O_5 1:2 sample, there is no trace of either $Hf_6Ta_2O_{17}$ or HfO_2. This indicates that Ta_2O_5 has a large solubility for HfO_2, which contradicts the proposed pseudobinary phase diagram. As noted above this point is under further study.

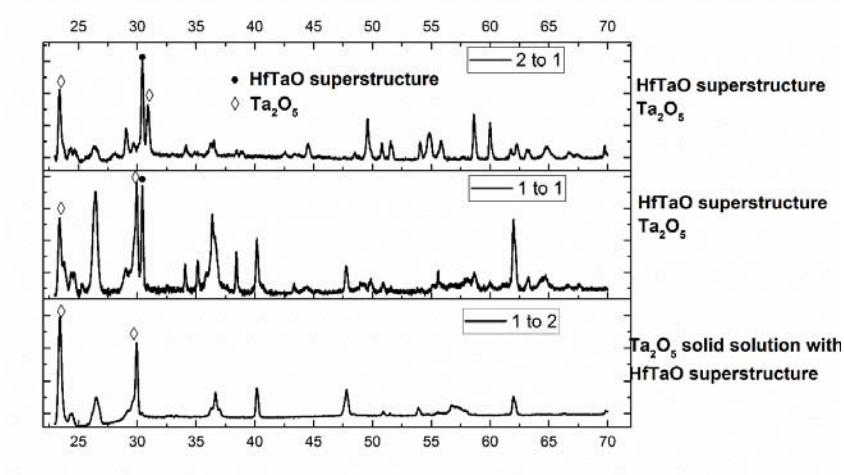

Fig. 18 XRD patterns for sinter mixed HfO_2 Ta_2O_5 samples with HfO_2:Ta_2O_5 ratio as 2:1, 1:1, 1:2.

7. Low thermal conductivity measurement

We have measured specific heat of HfTaO superstructure as shown in Fig. 19. In the figure , the black line represent the temperature profile during measurement, which is from room temperature to 1650°C, the blue and purple line is the baseline during the measurement, read line and green line is the signal from Al_2O_3, which is the standard sample and $Hf_6Ta_2O_{17}$ superstructure respectively. The specific heat is determined for the baselie offset between the sample and the alumina standard. From the DTA traces, the specific heat of HfTaO superstructure at 1650°C was calculated as 0.6358 $J/g^{-1}\cdot K^{-1}$, which is smaller than that of ZrO_2 (0.6675 $J/g^{-1}\cdot K^{-1}$

We also measured thermal conductivity on HfTaO superstructure directly. The thermal diffusivity and specific heat of the samples were measured from 25 to 1500 ºC at 100 ºC interval by the flash method using a NETZSCH LFA 427 instrument. This instrument and the test method conform to ASTM E1461-13, “Standard Test Method for Thermal Diffusivity by the Flash Method”.

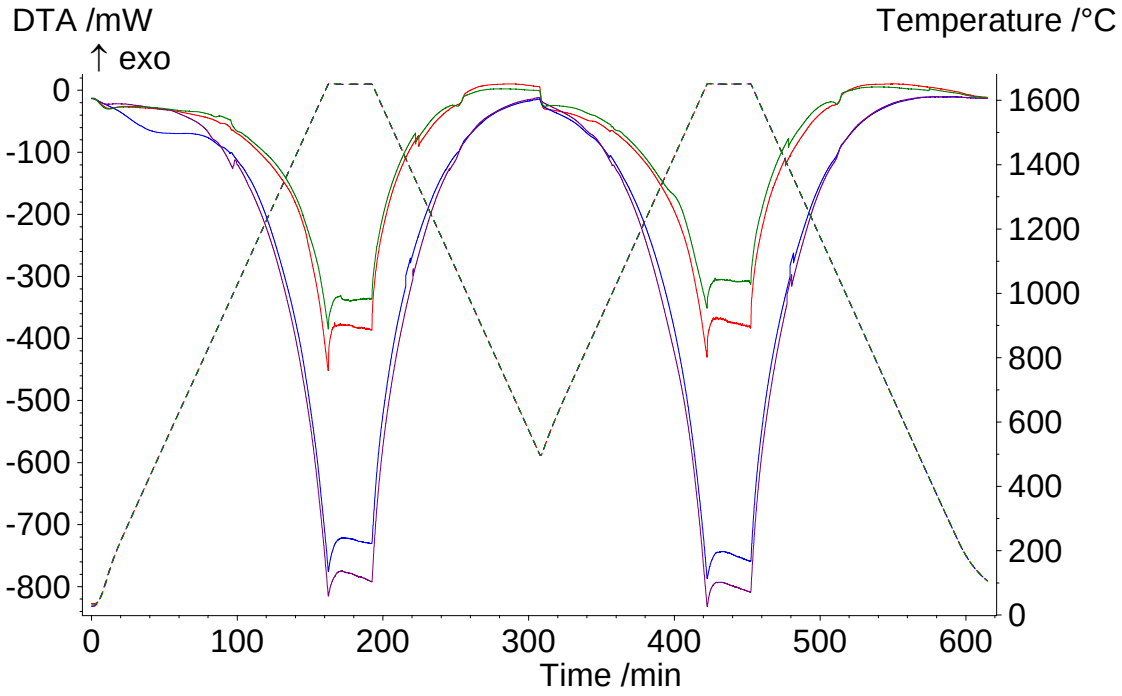

Fig. 19 DTA trace of HfTaO superstructure.

Transient heat transfer problems occur when the temperature distribution changes with time. The fundamental quantity that enters heat transfer situations not at steady-state is the thermal diffusivity. It is related to the steady-state thermal conductivity through the equation

$$D = \frac{K}{\rho C_p} \qquad 1$$

where
D = thermal diffusivity
K = thermal conductivity
Cp = specific heat
ρ = density

Thermal properties of materials are measured by experimentally establishing a heat flow boundary value problem, solving the theoretical equations, and then measuring the necessary temperatures or heat fluxes to determine the thermal property by matching to the theoretical solution. Thus, the easiest theoretical way to measure the thermal conductivity is to set up a steady-state, linear flow of heat through the material and apply Fourier's equation. This approach has led to the development of a number of methods for measuring the thermal conductivity including the guarded hot plate and linear rod methods. These methods are time consuming and can be susceptible to errors arising from non-realization of the assumed boundary or steady-state conditions. The flash methods of measuring thermal diffusivity remove the steady-state condition at the expense of measuring temperature as a varying function of time. The measurement of the thermal diffusivity of a material is usually carried out by rapidly heating one side of a

sample and measuring the temperature rise curve on the opposite side, as seen in Figure 20. The time that it takes for the heat to travel through the sample and cause the temperature to rise on the rear face can be used to determine the through-plane diffusivity. The through-plane thermal conductivity can then be calculated if the specific heat and density are known.

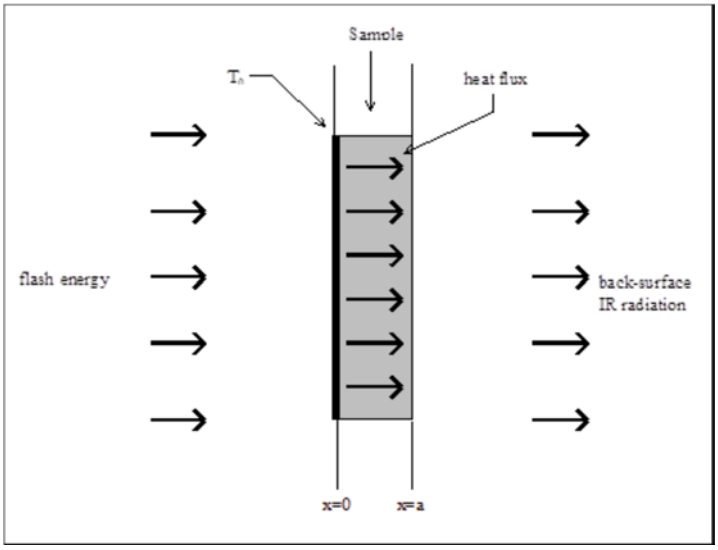

Figure 20 Illustration of the flash method for measuring thermal diffusivity.

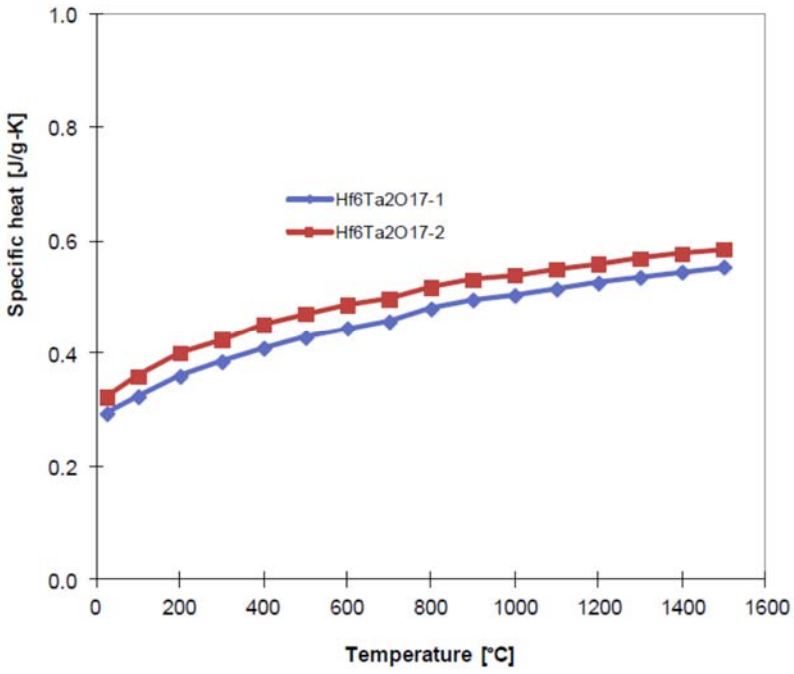

Figure 21 Specific heat as a function of temperature

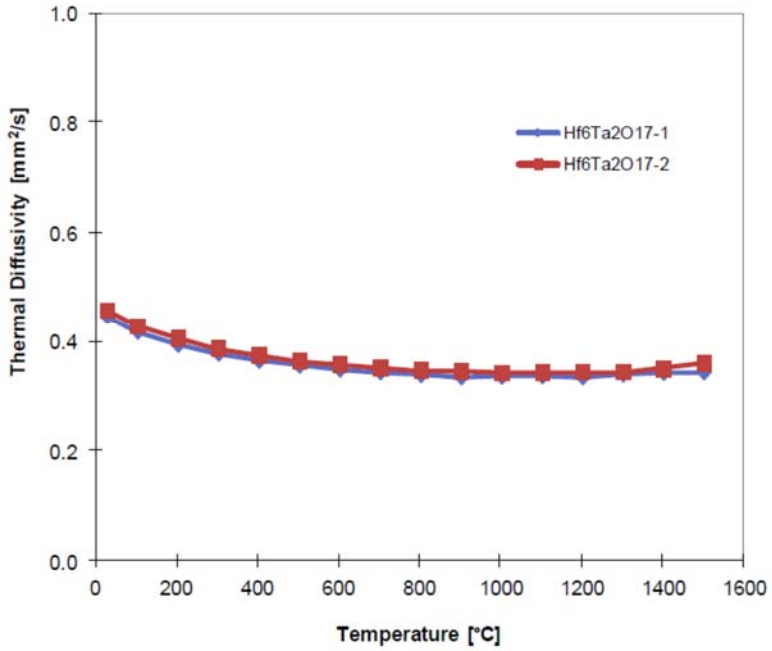

Figure 22 Temperature dependence of the thermal diffusivity

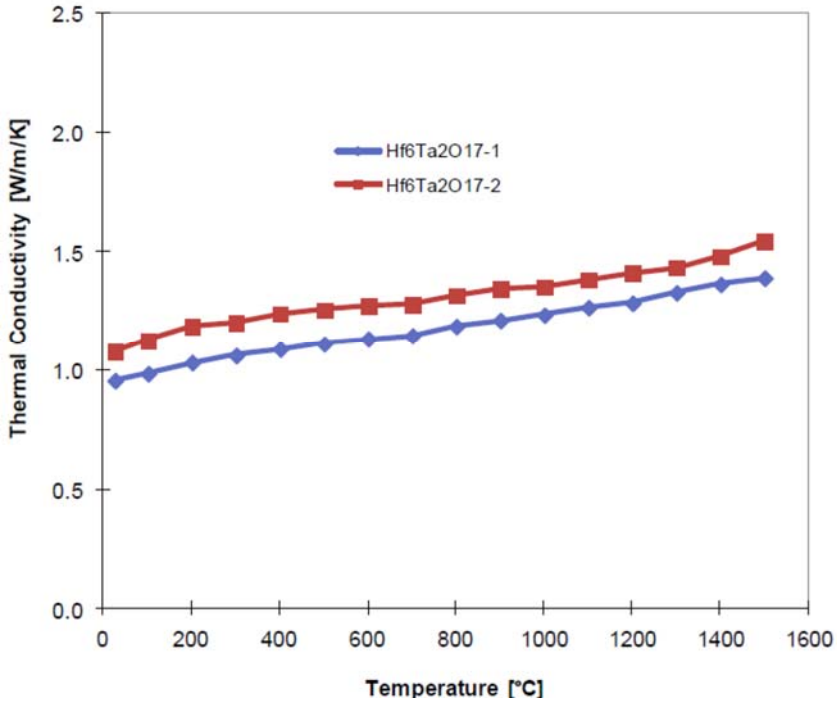

Figure 23 Temperature dependence of the thermal conductivity.

The final results indicate that the thermal conductivity of HfTaO is lower than that of cubic-ZrO_2, a well- known thermal barrier coating. This is being investigated further.

8. Oxidation kinetics of Hf-26.7Ta alloys coated by HfTaO superstructure

The oxidation kinetics shown in Fig. 24 were evaluated through TGA measurements at several temperatures. The Hf-26.7Ta alloy samples were oxidized at 1500°C to be coated with a layer of HfTaO protective layer. The oxidation kinetics exhibit a parabolic characteristic at first stage of oxidation (left to the vertical line shown in Fig. 24) and indicated decelerated oxidation speed. The second part of the kinetics can be fit to linear oxidation kinetics. This two mode oxidation kinetics is due to the crack and ablation at the corner of the sample (Fig. 25). Specifically it is evident from the Fig. 25 that sample corners are severely oxidized and sample at center is only modestly oxidized. This indicates that if the HfTaO coating can attach to substrate very well, it can be an effective protection coating. The similar oxidation kinetics at various temperature indicates that the good oxidation resistant properties of HfTaO superstructure can be used at a wide temperature range. Further study of the oxidation behavior is underway.

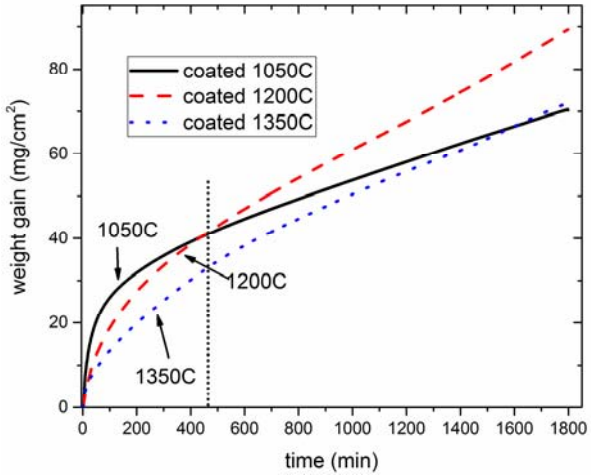

Fig. 24 Oxidation kinetics of Hf-26.7Ta alloy at several temperatures.

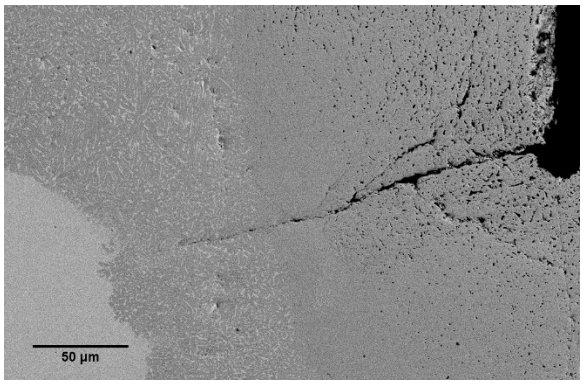

Fig. 25 Hf-26.7Ta alloy after TGA measurement with a right: corner crack..

Publication:

Yang, Y., J. H. Perepezko, and C. Zhang. "Oxidation synthesis of $Hf_6Ta_2O_{17}$ superstructures." *Materials Chemistry and Physics* 197 (2017): 154-162.

Reference

[AND12] A.-S. Andreani, A. Poulon-Quintin and F. Rebillat, Sur. Coat. Tech. Vol. 205 (2012) 1262-1267.

[KRI89] R. Krishnan, S.P. Garg and N. Krishnamurthy, "Hf-Ta (Hafnium-Tantalum)", Binary Phase Diagrams, 2114-2115 (ASM International, Materials Park, OH) (1989).

[MAR65] K. Marnoch, J. Met., vol.17 (11) (1965) 1225–1231.

[PER96] J.P. Perdew, K. Burke and M. Ernzerhof, Phys. Rev. Lett. Vol. 77 (1996) 3865-3868.

[RAM03] R. Ramprasad, J. Appl. Phy., vol. 94[9] (2003) 5609-5612.

[STR74] J. E. Stroud, W. C. Tripp and J.M. Wimmer, J. Am. Ceram. Soc., Vol. 57 (1974) 172-175.

[SPI81] F.M. Spiridonov, M.n. Mulenkova, V.I. Tsirel'nikov and L.N. Komissarova, Russ. J. Inorgan. Chem., vol. 26 (1981) 922-923.

[TER08] R. Terki, G. Bertrand, H. Aourag and C. Coddet, Materials Letters, vol. 62[10-11](2008) 1484-1486.